

# 3d transition metal impurities in diamond: electronic properties and chemical trends

L. V. C. Assali<sup>(1)</sup>, W. V. M. Machado<sup>(1)</sup>, and J. F. Justo<sup>(2)</sup>

<sup>(1)</sup> *Instituto de Física, Universidade de São Paulo,  
CP 66318, CEP 05315-970, São Paulo, SP, Brazil*

<sup>(2)</sup> *Escola Politécnica, Universidade de São Paulo,  
CP 61548, CEP 05424-970, São Paulo, SP, Brazil*

## Abstract

First principles calculations have been used to investigate the trends on the properties of isolated 3d transition metal impurities (from Sc to Cu) in diamond. Those impurities have small formation energies in the substitutional or double semi-vacancy sites, and large energies in the interstitial one. Going from Sc to Cu, the 3d-related energy levels in the bandgap move from the top of the bandgap toward the valence band in all three sites. Trends in electronic properties and transition energies of the impurities, in the substitutional or interstitial sites, are well described by a simple microscopic model considering the electronic occupation of the 3d-related levels. On the other hand, for the impurities in the double semi-vacancy site, there is a weak interaction between the divacancy- and the 3d-related orbitals, resulting in in vacancy- and 3d-related levels in the materials bandgap.

PACS numbers: 61.72.Bb, 71.55.-i, 71.55.Cn

## I. INTRODUCTION

Silicon-based device technology has flourished over the last four decades. In such a time span, miniaturization was the keyword for improving device performance. When new challenges were foreseen in the horizon, designers used to find new solutions to overcome them<sup>1</sup>. In a near future, intrinsic physical limits of this technology may preclude further improvements<sup>2</sup>. A different route for electronic devices could be the use of wide bandgap semiconductors<sup>3</sup>, since, when compared to silicon, they present superior materials properties for electronic devices, such as larger thermal conductivity, dielectric strength, and electron saturation velocity. There are still several technical limitations that prevent their competitiveness with the well established silicon technology. However, those materials have found their niche over the last decade, with applications in specific areas, such as high-power, high-temperature, high-frequency, opto-electronic<sup>4,5</sup>, and spintronic<sup>6,7</sup> devices.

There is currently a high demand for devices to operate under extreme conditions, and diamond is one of the leading candidates for such applications<sup>8-10</sup>. This material has a wide bandgap (experimental value of 5.5 eV), high saturated carrier velocities, high electric field breakdown strength, low dielectric constant, and high thermal conductivity. Synthetic diamond has been grown out of graphite by high pressure-high temperature methods for about fifty years<sup>11</sup> being currently the most widely used growing process that allows to get macroscopic diamond samples. In those processes, 3d transition metal (TM) alloys, involving mainly nickel, cobalt, and iron, are used as solvent-catalysts to both overcome the  $sp^2$  to  $sp^3$  energy barrier and accelerate the growth process<sup>12</sup>. Those TM end up being incorporated in the resulting diamond as residual impurities, either in isolated configurations or forming complexes with other defects, that can generate electrically and optically active centers<sup>12,13</sup>. Several transition metal-related active centers have been experimentally identified in diamond, and have been associated to impurities in substitutional, interstitial, or double semi-vacancy configurations<sup>13-16</sup>. Understanding the nature and microscopic structure of those centers is crucial in developing diamond-related technologies.

Here, we used first principles total energy calculations to investigate the electronic properties and chemical trends of 3d TM-related centers (from Sc to Cu) in diamond. We focused on the trends of impurities in the substitutional, interstitial, or double semi-vacancy sites. The stability of those defects, in all three sites, were computed in terms of their formation

energies. The electronic structure of this 3d<sup>n</sup> impurity family shows clear chemical trends in any site, with the 3d-related levels deepening from the top of the gap toward the valence band with increasing number (n) of 3d electrons. Additionally, we show that the respective electronic properties and transition energies could only be rationalized in terms of the number of electrons occupying the 3d-related energy levels within the materials bandgap.

## II. METHODOLOGY

The calculations were carried using the all-electron spin-polarized full-potential linearized augmented plane wave (FP-LAPW) method<sup>17</sup>, implemented in the WIEN2k package<sup>18</sup>. The electron-electron interactions were described within the framework of the density functional theory and the generalized gradient approximation<sup>19</sup>. Calculations were performed considering a 54-atom reference FCC supercell and a Monkhorst-Pack ( $2 \times 2 \times 2$ ) grid to sample the irreducible Brillouin zone<sup>20</sup>. Convergence on the total energy was achieved using a plane wave basis set to describe the interstitial region, with the set limited by the wave number  $7.0/R$ , where  $R = 1.2$  a.u. (0.635 Å) is the radius of all atomic spheres. Self-consistent iterations were performed until convergence on the total energy of  $10^{-4}$  Ry was achieved. In all systems with impurities, the internal degrees of freedom were optimized, without any symmetry constraints, until the force in each atom was smaller than  $10^{-3}$  Ry/a.u. Such theoretical framework and convergence criteria have been shown to provide a reliable description of the electronic properties of defect centers in several semiconductors<sup>21,22</sup>.

The formation energy of a TM impurity center in diamond ( $E_f^q$ ) was computed by<sup>13,21</sup>:

$$E_f^q = E_{tot}^q(N_C, N_{TM}) - N_C\mu_C - N_{TM}\mu_{TM} + q(\varepsilon'_v + \epsilon_F), \quad (1)$$

where  $E_{tot}^q(N_C, N_{TM})$  is the total energy of a supercell with the defect in a  $q$  charge state, with  $N_C$  carbon atoms and  $N_{TM}$  TM impurity atoms. The  $\mu_C$  and  $\mu_{TM}$  are the chemical potentials of respectively diamond and TM stable crystalline structures, computed within the same methodology described in the previous paragraph. Additionally,  $\epsilon_F$  is the Fermi energy ( $0 \leq \epsilon_F \leq \varepsilon_g$ , where  $\varepsilon_g$  is the bandgap energy) and  $\varepsilon'_v = \varepsilon_v + \delta_q$ , where  $\delta_q$  is a parameter that lines up the band structures of the bulk diamond material with and without the impurity in relation to the top of valence band of the pure crystal ( $\varepsilon_v$ ). Within our theoretical approximations, we found  $\varepsilon_g = 4.56$  eV for diamond.

For a certain impurity (in a substitutional, interstitial, or double semi-vacancy center), the transition energy between the  $q'$  and  $q$  charge states,  $E_t(q'/q)$ , is the value of the Fermi energy in the bandgap when the formation energies of the center in those respective charge states, as computed by equation 1, are equal.

$$E_t(q'/q) = \epsilon_F \quad \text{when} \quad E_f^{q'} - E_f^q = 0. \quad (2)$$

We should stress that here we computed the transition energies, not the excitation ones, in which other methodologies could be more appropriate<sup>23</sup>.

### III. RESULTS AND DISCUSSION

We computed the properties of the 3d transition metal impurities in diamond, from Sc (atomic configuration  $3d^1 4s^2$ ) to Cu (atomic configuration  $3d^{10} 4s^1$ ), in three different sites: tetrahedral interstitial ( $\text{TM}_i$ ), substitutional ( $\text{TM}_s$ ), and double semi-vacancy ( $\text{TM}_{2V}$ ) ones.

When a TM impurity, with a  $3d^n 4s^2$  ( $1 \leq n < 9$ ) atomic configuration, occupies a tetrahedral interstitial site in diamond ( $\text{TM}_i$ ), its 4s electrons are transferred to the 3d orbitals, resulting in a  $3d^{n+2}$  configuration. In a tetrahedral crystal field, the 3d states are split into  $e + t_2$  irreducible representations, with the threefold  $t_2$  states lying lower in energy than the two-fold  $e$  ones. This level ordering is the result of a strong octahedral crystal field created by the next nearest neighboring carbon atoms, that leads to a strong repulsion in the  $e$  states, moving them up, in the upper half of the bandgap. Additionally, the crystal field energy splitting ( $\Delta_{\text{CF}}^i$ ) is larger than the exchange splittings ( $\Delta_e^i$  and  $\Delta_t^i$ ), such that the system always presents a low spin configuration. This results from the small lattice parameter of diamond, and is consistent with TM impurities in boron nitride<sup>24</sup>. Figure 1(a) presents the specific case of  $\text{Mn}_i$  in the neutral charge state ( $3d^7$ ). For other  $\text{TM}_i$  impurities in diamond (from Sc to Cu), their  $t_2$  and  $e$  levels have an equivalent behavior to those of  $\text{Mn}_i$ , but with a chemical trend such that those levels move all together from the midgap region, in  $\text{Sc}_i$ , toward the valence band, in  $\text{Cu}_i$ , consistent with results for  $\text{TM}_i$  impurities in other semiconductors<sup>25,26</sup>. The 3d-character localization in the TM atomic spheres increases with increasing the atomic number.

In the substitutional site ( $\text{TM}_s$ ), the impurity presents a  $3d^{n-2}$  configuration, since four electrons are necessary for a covalent bonding with the four nearest neighboring carbon

atoms. In contrast to the interstitial case, the tetrahedral crystal field drives the  $e$  states to lie lower in energy than the  $t_2$  ones. Here, the crystal field splitting also prevails over the exchange splittings ( $\Delta_{\text{CF}}^s \gg \Delta_t^s$  and  $\Delta_e^s$ ). Figure 1(b) presents the specific case of  $\text{Mn}_s$  in the neutral charge state ( $3d^3$ ). For other  $\text{TM}_s$  impurities in diamond (from Sc to Cu), the  $e$  and  $t_2$  levels are equivalent to those of  $\text{Mn}_s$ , but with a chemical trend such that those levels move all together from the bandgap top, in  $\text{Sc}_s$ , toward the valence band, in  $\text{Cu}_s$ <sup>26</sup>. The 3d-character localization in the TM atomic spheres also increases with increasing the atomic number.

The electronic structure of the TM impurity in the double semi-vacancy site ( $\text{TM}_{2V}$ ) is considerably more complex than that in the other two sites. The electronic structure of  $\text{TM}_{2V}$  centers are result of an interaction between the divacancy states with the ones coming from the atomic TM, as represented in figure 1(c) for the  $\text{Mn}_{2V}$  center. The one-electron ground state structure of a diamond divacancy in  $D_{3d}$  symmetry has the  $e_u^2 e_g^0$  configuration in the bandgap region. In that symmetry, the TM 3d-related energy levels are split into  $2e_g + a_{1g}$ . When a TM atom is placed in the middle position of a divacancy, one of its  $e_g$  energy levels interacts slightly with the carbon dangling bonds, leaving a fully occupied non-bonding  $t_{2g}$ -like ( $e_g + a_{1g}$ ) orbital inside the valence band. However, the other TM-related  $e_g$  orbital interacts with the divacancy-related  $e_g$  gap state, resulting in an  $e_g$ -bonding level in the valence band and an  $e_g$ -anti-bonding one in the bandgap. The divacancy-related  $e_u$  orbitals do not interact with any 3d-related TM ones, and consequently they remain near the top of the valence band.

For the  $\text{TM}_{2V}$  center, depending on the impurity atomic number, the relative position of the 3d-related levels and the divacancy related ones may switch along the series, such that the electronic structure of each impurity depends strongly on such relative positions and the center charge state. Figure 2 presents the electronic structure of the  $\text{TM}_{2V}$ , in the neutral charge state. The figure presents, in parenthesis, the 3d character inside the TM atomic sphere of each energy level. Going from  $\text{Sc}_{2V}$  to  $\text{Cu}_{2V}$  impurity centers, the 3d- $t_{2g}$ -related levels move from the middle of the bandgap toward the valence band, crossing with the divacancy-related  $e_u$  ones, that lie near the valence band top. Additionally, the percentage of d-character increases along the series. These trends are consistent with those for substitutional and interstitial TM impurities. However, the electronic character of the highest occupied level of those centers depends on the relative position of the divacancy-

related levels with respect to the 3d-related ones. According to figure 2 for the  $\text{TM}_{2V}$  in the neutral charge state, it is associated to the TM for V, Fe, and Co, while it is associated to the divacancy for Sc, Ti, Cr, Mn, Ni, and Cu.

Figure 3 presents the trends on the formation energy for neutral impurities in all three sites, as computed by equation 1. The results show that the formation energies of a TM with  $3d^n$  or  $3d^{10-n}$  configurations are essentially equivalent in any site, with a clear energy favoring for the impurity in the middle of that family, which is manganese. Additionally, the interstitial site is the most unfavorable one for any TM, with formation energies of more than 10 eV higher than the respective ones in the other two sites<sup>22</sup>. The small energy difference for the impurity in the substitutional or double semi-vacancy sites suggests that those two configurations may compete, co-existing in the diamond samples. We should also stress that trends in energy differences between TM defects in interstitial and substitutional configurations remain essentially the same for defects in charge states other than neutral. Those trends in energy are consistent, for example, with available experimental data for concentrations of cobalt<sup>12</sup> and nickel<sup>13,16</sup> impurities in as-grown and annealed synthetic diamond.

Table I presents the local symmetry and spin of the relaxed configuration for the TM impurities in the neutral charge state. As result of the electronic structures, the  $\text{TM}_{2V}$  centers generally present spin values that are larger than the  $\text{TM}_i$  and  $\text{TM}_s$  centers. The manganese in the double semi-vacancy presents the largest spin of all centers ( $S=5/2$ ). This large spin value suggests potential applications for spintronic devices<sup>27,28</sup>.

Up to now, we have discussed the properties of the TM impurities in their neutral charge state. However, since those impurities introduce energy levels in the bandgap, both occupied and unoccupied ones, there is often a large number of possible stable charge states for each center. The transition energy between two different charge states is an important information for experimentalists to identify a certain center. Here, we carried out calculations for all stable charge states of each TM impurity in those three sites. Some centers presented up to seven different stable charge states, with transition energies lying in the diamond bandgap. The transition energy between two different charge states of a certain center was computed using the total energies of the centers in the initial and final charge states, as given by equations 1 and 2.

Our results indicated that the chemical trends on transition energies (computed by equa-

tion 2) along the 3d series, could only be rationalized if they were discussed in terms of the 3d-related level occupation and the respective crystal field and exchange splittings, as presented in figure 1. The comparison among different TM impurities should be conducted considering the same number of total electrons in each system, as discussed below. The transition energies within the diamond bandgap for  $\text{TM}_s$  (from Sc to Cu) are shown in figure 4. The stable charge state of a certain center depends on the position of the Fermi level in the bandgap. For example, the  $\text{Ti}_s$  presents two transition states in the bandgap, the (0/-) and (-/2-), as shown in figure 4. This means that this center is stable in the neutral charge state for  $0 < \epsilon_F \leq 3.0$  eV, in the negatively charge state for  $3.0 \leq \epsilon_F \leq 3.8$  eV, and in the double negatively charge state for  $3.8 \text{ eV} \leq \epsilon_F < \epsilon_g$ .

According to figure 1(b), the  $\text{TM}_s$  impurity centers introduce energy levels with  $e$  and  $t_2$  irreducible representations, with  $e_\uparrow$  and  $e_\downarrow$  states below  $t_{2\uparrow}$  and  $t_{2\downarrow}$  ones. For an impurity with a  $3d^n 4s^2$  atomic configuration, those levels are filled with  $(n - 2)$ d-electrons. For  $\text{Sc}_s^-$  center ( $n = 2$ ), the  $e$  and  $t_2$  states are empty and the bandgap electronic configuration is  $e_\uparrow^0 e_\downarrow^0 t_{2\uparrow}^0 t_{2\downarrow}^0$ , where the level ordering is consistent with the increasing values of the respective energy eigenvalues, as given in figure 1(b). The  $\text{Sc}_s^{2-}$  center is related to adding one electron to an unoccupied  $e$  level, leading to the  $e_\uparrow^1 e_\downarrow^0 t_{2\uparrow}^0 t_{2\downarrow}^0$  bandgap electronic configuration. Therefore, the (-/2-) transition state is described by the connection between initial and final electronic configurations, as represented by  $e_\uparrow^0 e_\downarrow^0 t_{2\uparrow}^0 t_{2\downarrow}^0 \rightarrow e_\uparrow^1 e_\downarrow^0 t_{2\uparrow}^0 t_{2\downarrow}^0$ . It could be represented in a compact form as  $e^0 \rightarrow e^1$ , or just  $[e^0/e^1]$  in figure 4. Accordingly, the (2 - /3-) transition state, or  $[e^1/e^2]$ , is related to the  $e^1 \rightarrow e^2$  electronic configurations. For  $\text{Sc}_s$ , there is no additional transition state that lies in the bandgap.

For  $\text{Ti}_s$ , the (0/-) and (-/2-) transition states are associated with  $e_\uparrow^0 \rightarrow e_\uparrow^1$  and  $e_\uparrow^1 \rightarrow e_\uparrow^2$  electronic configurations, respectively. Those two transition states should be compared respectively to the (-/2-) e (2 - /3-) transition ones of  $\text{Sc}_s$  center, that is why the transitions are connected by lines, as a guide to the eye, in figure 4. Going to  $\text{V}_s$ , the same electronic configurations are observed, being now related to the (+/0) and (0/-) transition energies. However, the  $\text{V}_s$  center carried more two possible electronic configurations in the diamond bandgap, related to  $\text{V}_s^{2-}$  and  $\text{V}_s^{3-}$  centers, allowing to compute the transition energies between the electronic configurations  $e_\uparrow^2 e_\downarrow^0 t_{2\uparrow}^0 t_{2\downarrow}^0 \rightarrow e_\uparrow^2 e_\downarrow^1 t_{2\uparrow}^0 t_{2\downarrow}^0$  (or in a compact form,  $e^2 \rightarrow e^3$ ) and  $e^3 \rightarrow e^4$ , associated with the (-/2-) and (2 - /3-) transition states, respectively. The  $\text{Mn}_s$  impurity has four stable charge states in the bandgap. For this impurity, after the  $e_\uparrow$  and

$e_{\downarrow}$  states are fully occupied, additional electrons could only occupy the  $t_2$  states. For  $Mn_s$ , there is the  $e^4 t_{2\uparrow}^0 t_{2\downarrow}^0 \rightarrow e^4 t_{2\uparrow}^1 t_{2\downarrow}^0$  transition, associated with the  $(-/2-)$  one. From  $Co_s$  to  $Cu_s$ , there are  $e^4 t_{2\uparrow}^0 t_{2\downarrow}^0 \rightarrow e^4 t_{2\uparrow}^1 t_{2\downarrow}^0$ ,  $e^4 t_{2\uparrow}^1 t_{2\downarrow}^0 \rightarrow e^4 t_{2\uparrow}^2 t_{2\downarrow}^0$ ,  $e^4 t_{2\uparrow}^2 t_{2\downarrow}^0 \rightarrow e^4 t_{2\uparrow}^3 t_{2\downarrow}^0$ , and  $e^4 t_{2\uparrow}^3 t_{2\downarrow}^0 \rightarrow e^4 t_{2\uparrow}^3 t_{2\downarrow}^1$  (or  $t_2^3 \rightarrow t_2^4$ ) transitions. Therefore, one could associate, for example, the  $(-/2-)$  transition of  $Sc_s$  with the  $(0/-)$  one of  $Ti_s$  and the  $(+/0)$  of  $V_s$ , i.e. transitions that involve the same number of electrons in the system. For all those centers, it is observed that any transition state has a chemical trend to move from the top of the bandgap in Sc toward the valence band maximum in Cu. Such trend is result of a Coulomb interaction, since the increasing atomic number, with a constant number of electrons, increases the nuclei-electron attractive interaction, reducing the total energy of the system.

Those results allow to establish a microscopic model for a transition energy, associated with the 3d level occupation in the bandgap. There is a small energy difference between the  $e^0 \rightarrow e^1$  and  $e^1 \rightarrow e^2$  transitions, which is associated with the occupation of the  $e_{\uparrow}$ , being result of a Coulomb interaction. Now, there is a large energy difference between  $e^1 \rightarrow e^2$  and  $e^2 \rightarrow e^3$  transitions, which results from the exchange potential splitting ( $\Delta_e^s$ ). This is because the  $e^2 \rightarrow e^3$  transition differs from the  $e^1 \rightarrow e^2$  one by the addition of an electron with a different spin. The large energy difference between the  $e^3 \rightarrow e^4$  and  $t_2^0 \rightarrow t_2^1$  transitions results from the presence of a strong crystal field splitting ( $\Delta_{CF}^s$ ), which is larger than the exchange potential splittings ( $\Delta_e^s$  and  $\Delta_t^s$ ). For the transitions related to the occupation of the  $t_{2\uparrow}$  state (up to 3 electrons), the small energy difference is result of a Coulomb interaction. Finally, for the  $t_2^3 \rightarrow t_2^4$  transition, the large energy difference is controlled by the exchange potential splitting of the  $t_2$  state ( $\Delta_t$ ).

The same model could be used to discuss the transition energies associated with TM impurities in the interstitial site, as presented in figure 5. According to figure 1(a), the  $TM_i$  centers introduce energy levels with  $t_2$  and  $e$  irreducible representations in the bandgap, with  $t_{2\uparrow}$  and  $t_{2\downarrow}$  states below the  $e_{\uparrow}$  and  $e_{\downarrow}$  ones. For an impurity with a  $3d^n 4s^2$  atomic configuration, those levels are filled with  $(n+2)$ d-electrons. The first possible transition energy is associated to the electronic initial and final configurations  $t_{2\uparrow}^0 t_{2\downarrow}^0 e_{\uparrow}^0 e_{\downarrow}^0 \rightarrow t_{2\uparrow}^1 t_{2\downarrow}^0 e_{\uparrow}^0 e_{\downarrow}^0$ . It could be represented in a compact form as  $t_2^0 \rightarrow t_2^1$ , or just  $[t_2^0/t_2^1]$  in figure 5. Those configurations are associated with the  $(3+/2+)$  and  $(4+/3+)$  transition states for the  $Sc_i$  and  $Ti_i$  impurities, respectively. After all the  $t_2$  states are filled with increasing Fermi energy, the large energy difference for the  $t_2^6 e_{\uparrow}^0 e_{\downarrow}^0 \rightarrow t_2^6 e_{\uparrow}^1 e_{\downarrow}^0$  electronic configurations (or in compact

form  $e^0 \rightarrow e^1$ ) is associated with the crystal field splitting ( $\Delta_{\text{CF}}^i$ ), consistent with the model of figure 1. For all those centers, it is observed that any transition state, along the 3d series, has a chemical trend to move from the upper half region of the bandgap, in Sc, toward the valence band maximum, in Cu. Additionally, the crystal field splitting for the  $\text{TM}_i$  centers is considerably smaller than the respective splitting for the  $\text{TM}_s$  ones ( $\Delta_{\text{CF}}^i \ll \Delta_{\text{CF}}^s$ ).

For the  $\text{TM}_{2V}$ , this model could be applied only to a few transition states, since the almost non-interacting divacancy-related energy levels and the 3d-related ones lie in the same region of the bandgap, as shown in figure 2. As mentioned earlier, the divacancy-related states ( $e_u$ ) remain in the bottom of the bandgap, the 3d-related states ( $e_g + a_{1g}$ ) move from the top of the gap in Sc toward the valence band in Cu. While some transition states are computed in association with electronic configurations filling the divacancy-related states, others are associated with filling the TM-related states. The transition energies associated with the  $\text{TM}_{2V}$  centers are presented in figure 6. The trends can be here observed for some TM impurities. On the other hand, the V, Fe, and Co are exceptions, since the highest occupied level in their neutral charge state has a 3d-related character, as shown in figure 2. For those cases, the electronic configurations are considerably richer, which are presented in table II for several charge states. Therefore, table II helps to assign the electronic configurations associated with the respective transitions. According to figure 6, in general, transition energies related to occupying the divacancy-related orbitals ( $e_u$ ) are in the lower part of the bandgap while transition states associated to occupying the 3d-related states ( $e_g$  and  $a_{1g}$ ) are mostly in the upper part of the bandgap.

#### IV. SUMMARY

In summary, we have investigated the electronic properties and chemical trends of isolated 3d-transition metal impurities in diamond. We have shown that impurities in the substitutional or double semi-vacancy centers have smaller formation energies than the isolated centers in the interstitial site. We have also shown that trends on transition energies, for any of the three sites, could only be rationalized if they were discussed in terms of the increasing occupation of 3d-related states in the bandgap. Such trends are consistent with what would be expected for transition metal impurities in other semiconductors in either

isolated configurations<sup>29,30</sup> or forming complexes with other defects<sup>25,31</sup>.

**Acknowledgments:** The authors acknowledge support from Brazilian agencies CNPq and FAPESP. The calculations were performed in part using the computational facilities of the CENAPAD and the LCCA-CCE of the University of São Paulo.

- 
- <sup>1</sup> M. Schulz, *Nature (London)* **399**, 729 (1999).
  - <sup>2</sup> R. W. Keyes, *Rep. Prog. Phys.* **68**, 2701 (2005).
  - <sup>3</sup> V. V. Buniatyan and V. M. Aroutiounian, *J. Phys. D* **40**, 6355 (2007).
  - <sup>4</sup> Y. Gurbuz, O. Esame, I. Tekin, W. P. Kang, and J. L. Davidson, *Solid State Electr.* **49**, 1055 (2005).
  - <sup>5</sup> *Wide Bandgap Semiconductors: Fundamental Properties and Modern Photonic and Electronic Devices*, eds. K. Takahashi, A. Yoshikawa, and A. Sandhu (Springer, Berlin, 2007).
  - <sup>6</sup> M. V. G. Dutt, L. Childress, L. Jiang, E. Togan, J. Maze, F. Jelezko, A. S. Zibrov, P. R. Hemmer, and M. D. Lukin, *Science* **316**, 1312 (2007).
  - <sup>7</sup> A. A. Khajetoorians, B. Chilian, J. Wiebe, S. Schuwalow, F. Lechermann, and R. Wiesendanger, *Nature (London)* **467**, 1084 (2010).
  - <sup>8</sup> J. L. Hudgins, G. S. Simin, E. Santi, and M. A. Khan, *IEEE Trans. Power Electr.* **18**, 907 (2003).
  - <sup>9</sup> R. J. Nicholas, A. Mainwood, and L. Eaves, *Philos. Trans. Royal Soc. A - Math. Phys. Eng. Sci.* **366**, 189 (2008).
  - <sup>10</sup> C. J. H. Wort and R. S. Balmer, *Mater. Today* **11**, 22 (2008).
  - <sup>11</sup> F. P. Bundy, H. T. Hall, H. M. Strong and R. H. Wentorf, *Nature (London)* **176**, 51 (1955).
  - <sup>12</sup> A. Yelisseyev and H. Kanda, *New Diam. Front. Carbon Tech.* **17**, 127 (2007).
  - <sup>13</sup> R. Larico, J. F. Justo, W. V. M. Machado, and L. V. C. Assali, *Phys. Rev. B* **79**, 115202 (2009).
  - <sup>14</sup> A. T. Collins, *Diamond Relat. Mater.* **9**, 417 (2000).
  - <sup>15</sup> K. Iakoubovskii and A. T. Collins, *J. Phys.: Condens. Matter* **16**, 6897 (2004).
  - <sup>16</sup> V. A. Nadolinny, J. M. Baker, O. P. Yuryeva, M. E. Newton, D. J. Twitchen, and Y. N. Palyanov, *Appl. Magn. Reson.* **28**, 365 (2005).
  - <sup>17</sup> D. J. Singh, *Planewaves, Pseudopotentials and the LAPW method* (Kluwer Academic, Norwell,

- 1994).
- <sup>18</sup> P. Blaha, K. Schwarz, G. Madsen, D. Kvaniscka, and J. Luitz, in *WIEN2k, An Augmented Plane Wave Plus Local Orbitals Program for Calculating Crystal Properties*, edited by K. Schwarz (Technical Universität Wien, Austria, 2001).
- <sup>19</sup> J. P. Perdew, K. Burke, and M. Ernzerhof, *Phys. Rev. Lett.* **77**, 3865 (1996).
- <sup>20</sup> H. J. Monkhorst and J. D. Pack, *Phys. Rev. B* **13**, 5188 (1976).
- <sup>21</sup> L. V. C. Assali, W. V. M. Machado, and J. F. Justo, *Phys. Rev. B* **69**, 155212 (2004).
- <sup>22</sup> R. Larico, L. V. C. Assali, W. V. M. Machado, and J. F. Justo, *Appl. Phys. Lett.* **84**, 720 (2004).
- <sup>23</sup> T. V. Albu, A. B. Anderson, and J. C. Angus, *J. Electrochem. Soc.* **149**, E143 (2002).
- <sup>24</sup> L. V. C. Assali, W. V. M. Machado, and J. F. Justo, *Appl. Phys. Lett.* **89**, 072102 (2006).
- <sup>25</sup> L. V. C. Assali and J. F. Justo, *Phys. Rev. B* **58**, 3870 (1998).
- <sup>26</sup> L. V. C. Assali, W. V. M. Machado, and J. F. Justo, *Physica B* **404**, 4515 (2009).
- <sup>27</sup> T. Jungwirth, J. Sinova, J. Masek, K. Kucera, and A. H. MacDonald, *Rev. Mod. Phys.* **78**, 809 (2006).
- <sup>28</sup> E. B. Lombardi, *Diam. Relat. Mater.* **17**, 1345 (2008).
- <sup>29</sup> H. Raebiger, S. Lany, and A. Zunger, *Phys. Rev. B* **79**, 165202 (2009).
- <sup>30</sup> A. Continenza, G. Profeta, and S. Picozzi, *Phys. Rev. B* **73**, 035212 (2006).
- <sup>31</sup> S. Zhao, L. V. C. Assali, J. F. Justo, G. H. Gilmer, and L. C. Kimerling, *J. Appl. Phys.* **90**, 2744 (2001).

TABLE I: Point symmetry and spin (S) 3d TM impurities in the neutral charge state. The table presents results for interstitial, substitutional and double semi-vacancy sites.

Site		Sc	Ti	V	Cr	Mn	Fe	Co	Ni	Cu
TM <sub>i</sub>	Sym.	T <sub>d</sub>	D <sub>2d</sub>	D <sub>2</sub>	T <sub>d</sub>	D <sub>2d</sub>	T <sub>d</sub>	D <sub>2d</sub>	T <sub>d</sub>	D <sub>2d</sub>
	S	3/2	0	1/2	0	1/2	1	1/2	0	1/2
TM <sub>s</sub>	Sym.	D <sub>2d</sub>	T <sub>d</sub>	D <sub>2d</sub>	T <sub>d</sub>	D <sub>2d</sub>	T <sub>d</sub>	D <sub>2d</sub>	C <sub>1</sub>	T <sub>d</sub>
	S	1/2	0	1/2	1	1/2	0	1/2	1	3/2
TM <sub>2V</sub>	Sym.	C <sub>2h</sub>	D <sub>3d</sub>	D <sub>3d</sub>	C <sub>2h</sub>	D <sub>3d</sub>	D <sub>3d</sub>	C <sub>2h</sub>	D <sub>3d</sub>	C <sub>i</sub>
	S	3/2	1	3/2	2	5/2	2	3/2	1	1/2

TABLE II: Electronic configuration (EC), for the divacancy-related and TM 3d-related energy levels, and spin (S) for the  $\text{TM}_{2V}^q$  centers in diamond in  $q$  charge state, with  $\text{TM} = \text{V}, \text{Fe}, \text{and Co}$ .

$q$	$\text{V}_{2V}$		$\text{Fe}_{2V}$		$\text{Co}_{2V}$	
	EC	S	EC	S	EC	S
2+	—	—	—	—	$e_{g\uparrow}^2 a_{1g\uparrow}^1 a_{1g\downarrow}^1 e_{u\uparrow}^1 e_{g\downarrow}^0 e_{u\downarrow}^0$	3/2
+	$e_{u\uparrow}^2 a_{1g\uparrow}^0 e_{g\uparrow}^0 a_{1g\downarrow}^0 e_{u\downarrow}^0 e_{g\downarrow}^0$	1	$a_{1g\uparrow}^1 e_{g\uparrow}^2 e_{u\uparrow}^2 a_{1g\downarrow}^0 e_{g\downarrow}^0 e_{u\downarrow}^0$	5/2	$e_{g\uparrow}^2 a_{1g\uparrow}^1 a_{1g\downarrow}^1 e_{u\uparrow}^2 e_{g\downarrow}^0 e_{u\downarrow}^0$	2
0	$e_{u\uparrow}^2 a_{1g\uparrow}^1 e_{g\uparrow}^0 e_{u\downarrow}^0 e_{g\downarrow}^0 a_{1g\downarrow}^0$	3/2	$e_{g\uparrow}^2 a_{1g\uparrow}^1 e_{u\uparrow}^2 a_{1g\downarrow}^0 e_{u\downarrow}^0 e_{g\downarrow}^0$	2	$e_{g\uparrow}^2 a_{1g\uparrow}^1 a_{1g\downarrow}^1 e_{u\uparrow}^2 e_{g\downarrow}^1 e_{u\downarrow}^0$	3/2
-	$e_{u\uparrow}^2 a_{1g\uparrow}^1 e_{u\downarrow}^1 e_{g\uparrow}^0 e_{g\downarrow}^0 a_{1g\downarrow}^0$	1	$e_{g\uparrow}^2 a_{1g\uparrow}^1 e_{u\uparrow}^2 a_{1g\downarrow}^1 e_{u\downarrow}^1 e_{g\downarrow}^0$	3/2	$e_{u\uparrow}^2 a_{1g\uparrow}^1 a_{1g\downarrow}^1 e_{g\uparrow}^2 e_{g\downarrow}^2 e_{u\downarrow}^0$	1
2-	$e_{u\uparrow}^2 e_{u\downarrow}^2 a_{1g\uparrow}^1 e_{g\uparrow}^0 e_{g\downarrow}^0 a_{1g\downarrow}^0$	1/2	$e_{g\uparrow}^2 a_{1g\uparrow}^1 e_{u\uparrow}^2 e_{u\downarrow}^2 a_{1g\downarrow}^1 e_{g\downarrow}^0$	1	$e_{u\uparrow}^2 a_{1g\uparrow}^1 a_{1g\downarrow}^1 e_{g\uparrow}^2 e_{g\downarrow}^2 e_{u\downarrow}^1$	1/2
3-	$e_{u\uparrow}^2 e_{u\downarrow}^2 e_{g\uparrow}^2 a_{1g\uparrow}^0 a_{1g\downarrow}^0 e_{g\downarrow}^0$	1	$e_{g\uparrow}^2 e_{u\uparrow}^2 e_{u\downarrow}^2 a_{1g\uparrow}^1 e_{g\downarrow}^2 a_{1g\downarrow}^0$	1/2	$e_{u\uparrow}^2 e_{u\downarrow}^2 a_{1g\uparrow}^1 a_{1g\downarrow}^1 e_{g\uparrow}^2 e_{g\downarrow}^2$	0
4-	$e_{u\uparrow}^2 e_{u\downarrow}^2 e_{g\uparrow}^2 a_{1g\uparrow}^1 e_{g\downarrow}^0 a_{1g\downarrow}^0$	3/2	$e_{u\uparrow}^2 e_{u\downarrow}^2 a_{1g\uparrow}^1 a_{1g\downarrow}^1 e_{g\uparrow}^2 e_{g\downarrow}^2$	0	—	—

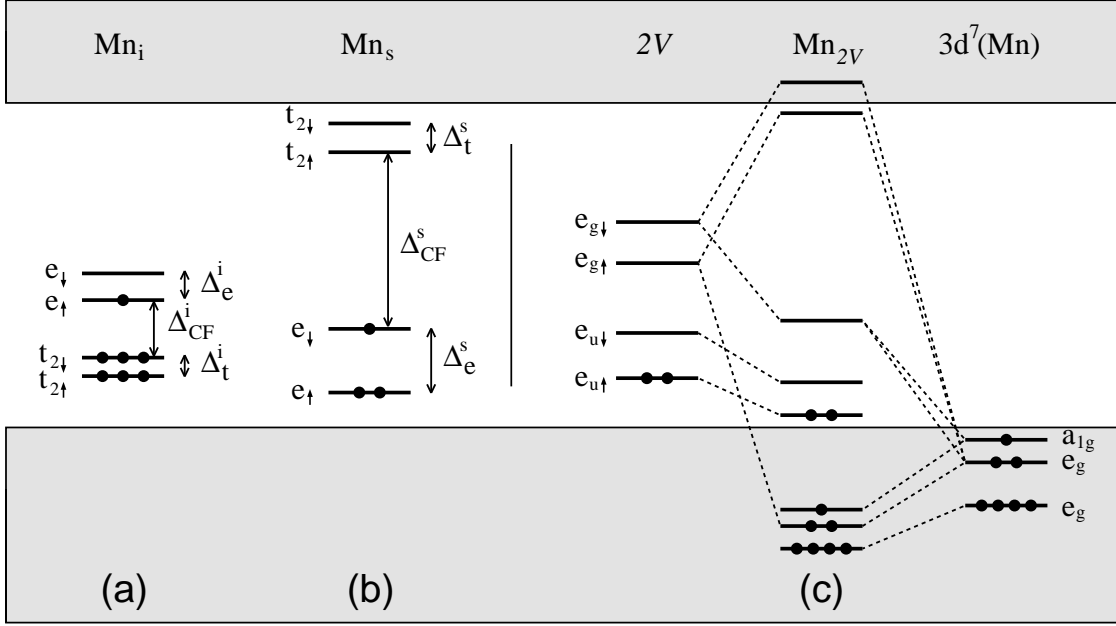


FIG. 1: Schematic representation of the gap energy electronic states for a manganese impurity in (a) interstitial (Mn<sub>i</sub>), (b) substitutional (Mn<sub>s</sub>) and (c) double semi-vacancy (Mn<sub>2V</sub>) sites. In the case of (Mn<sub>2V</sub>), the figure presents the model of a hybridization between the divacancy states (2V) and the 3d electrons in an isolated atomic configuration (Mn). The ↑ and ↓ arrows represent the spin up and down, respectively. Gray regions represent the diamond valence and conduction bands. For simplicity, the systems are represented considering a tetrahedral symmetry, neglecting symmetry lowering distortions. For Mn<sub>i</sub> (Mn<sub>s</sub>), the figure presents the exchange potential splittings Δ<sub>e</sub><sup>i</sup> and Δ<sub>t</sub><sup>i</sup> (Δ<sub>e</sub><sup>s</sup> and Δ<sub>t</sub><sup>s</sup>) and the crystal field splitting Δ<sub>CF</sub><sup>i</sup> (Δ<sub>CF</sub><sup>s</sup>).

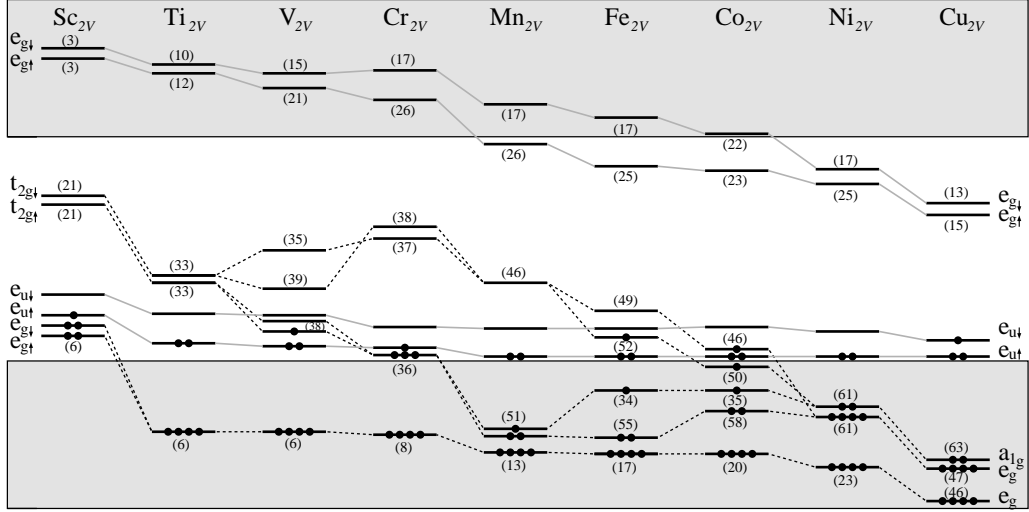


FIG. 2: The energy eigenvalues representing the divacancy- and TM  $3d$ -related levels in the gap region for the  $TM_{2V}$  centers ( $TM = Sc, Ti, V, Cr, Mn, Fe, Co, Ni,$  and  $Cu$ ). Levels with spin up and down are represented by  $\uparrow$  and  $\downarrow$  arrows, respectively. The filled (open) circles represent the electronic (hole) occupation of the gap levels. Numbers in parenthesis represent the  $d$ -character percentage of charge inside the TM atomic spheres. Level labeling is consistent with the model presented in Fig. 1(c). For clarity, the results presented in the figure corresponded to a high-symmetry  $D_{3d}$  configuration, although the converged calculations took no symmetry constraints, as presented in Table I. Levels associated to the TM (divacancy) are connected by dashed (full gray) lines.

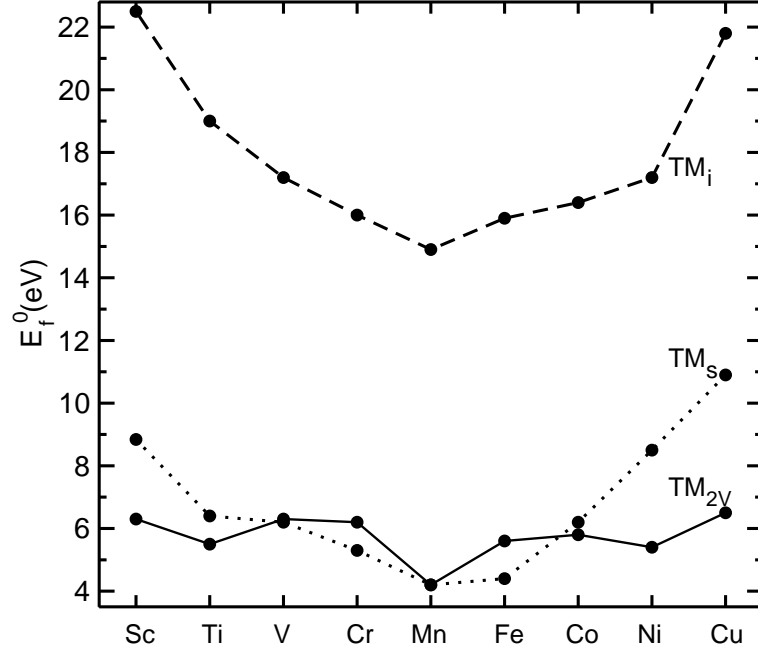


FIG. 3: Formation energy of the 3d TM impurities, in the neutral charge state ( $E_f^0$ ), in substitutional (dotted line), interstitial (dashed line), and double semi-divacancy (full line) sites.

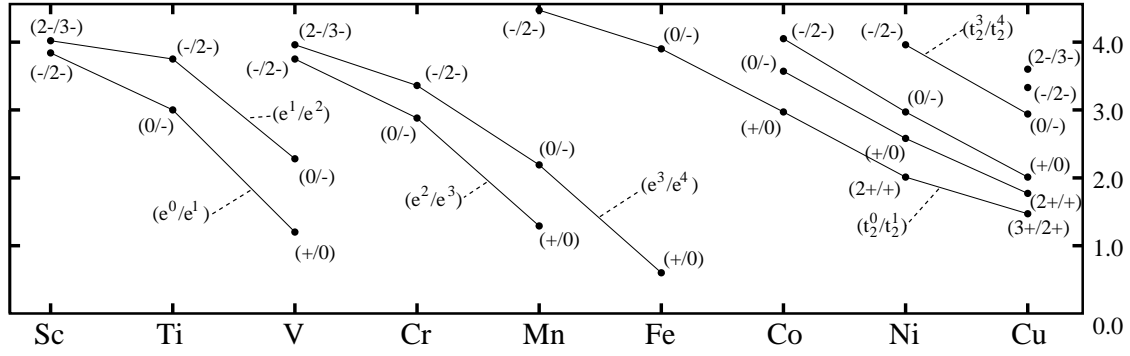


FIG. 4: Transition energies ( $E_t$ ) of 3d TM impurities in the substitutional site. The initial and final 3d-related bandgap electronic configurations are given in square brackets (see text). The lines in the figure are only guides to the eye, connecting different transition states related with the same electronic configurations of different TM impurities.

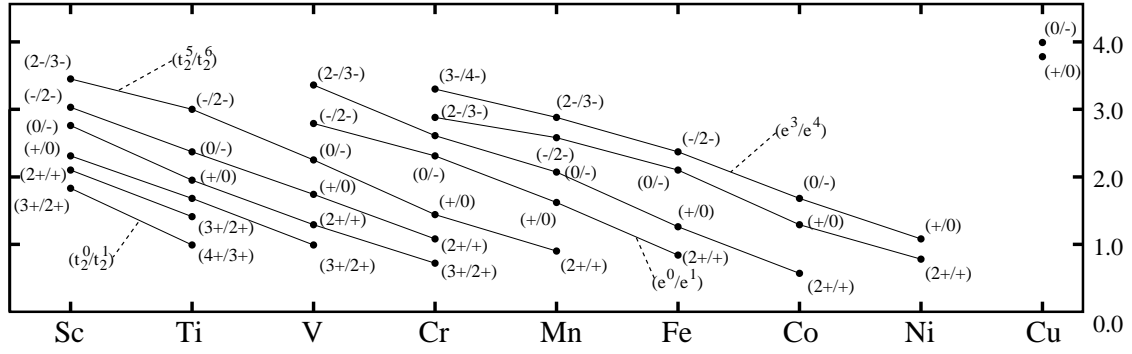


FIG. 5: Transition energies ( $E_t$ ) of 3d TM impurities in the interstitial site. The lines and symbols are consistent with the ones in figure 4.

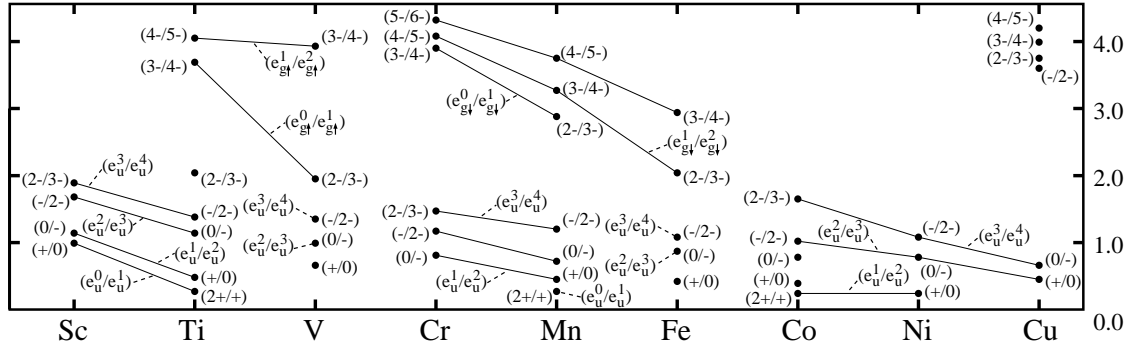


FIG. 6: Transition energies ( $E_t$ ) of 3d TM impurities in the double semi-vacancy site. The lines and symbols are consistent with the ones in figure 4.